

# SUPPLEMENTARY MATERIALS OF LOW-LIGHT IMAGE ENHANCEMENT VIA WEIGHTED LOW-RANK TENSOR REGULARIZED RETINEX MODEL

Weipeng Yang<sup>1</sup>, Hongxia Gao<sup>1,2\*</sup>, Wenbin Zou<sup>1</sup>, Shasha Huang<sup>1</sup>, Hongsheng Chen<sup>1</sup>, Jianliang Ma<sup>1,3</sup>

<sup>1</sup>School of Automation Science and Engineering, South China University of Technology, Guangzhou, China

<sup>2</sup>Research Center for Brain-Computer Interface, Pazhou Laboratory, Guangzhou, China

<sup>3</sup>KUKA Robotics Guangdong Co., Ltd., Foshan, China

## 1. NOTATIONS AND PRELIMINARIES

A tensor can be treated as a multi-indexed array, with its order determined by the number of dimensions or modes. In this paper, a tensor of  $N$ -order is denoted by Euler script letter, e.g.,  $\mathcal{X} \in \mathbb{R}^{I_1 \times I_2 \times \cdots \times I_N}$  and its entries by  $x_{i_1 i_2 \cdots i_N}$ . A matrix is a tensor of 2-order, denoted by boldface capital letter, e.g.,  $\mathbf{X}$ , and a vector is a tensor of 1-order, denoted as  $\mathbf{x}$ .

**Definition 1 (Mode-n Multiplication)** [1] The mode-n multiplication of a tensor  $\mathcal{X} \in \mathbb{R}^{I_1 \times I_2 \times \cdots \times I_N}$  with a matrix  $\mathbf{U} \in \mathbb{R}^{J \times I_n}$  is denoted by  $\mathcal{X} \times_n \mathbf{U}$  and is of size  $I_1 \times \cdots I_{n-1} \times J \times I_{n+1} \times \cdots \times I_N$ . Elementwise, we have  $(\mathcal{X} \times_n \mathbf{U})_{i_1 \cdots i_{n-1} j i_{n+1} \cdots i_N} = \sum_{i_n=1}^{I_n} x_{i_1 i_2 \cdots i_N} u_{j i_n}$ .

**Definition 2 (Tucker Decomposition)** [1][2] The tucker decomposition is a form of high order singular value decomposition (HOSVD), which decomposes a tensor into a core tensor multiplied by a matrix along each mode. Thus, in the 3-order case where  $\mathcal{X} \in \mathbb{R}^{I_1 \times I_2 \times I_3}$ , we have

$$\mathcal{X} = \mathcal{S} \times_1 \mathbf{U}_1 \times_2 \mathbf{U}_2 \times_3 \mathbf{U}_3, \quad (1)$$

where  $\mathbf{U}_i \in \mathbb{R}^{I_i \times I_i}$  is the column-wise orthogonal factor matrix and can be thought of as the principal component in the  $i$ -th mode,  $\mathcal{S} \in \mathbb{R}^{I_1 \times I_2 \times I_3}$  is the core tensor and its entries show the level of interaction between the different components. For more details on tensor notations, please refer to [1, 2].

## 2. WEIGHTED LOW-RANK TENSOR REGULARIZATION

Low-rank matrix approximation is a technique widely used in computer vision to recover an underlying low-rank matrix from a degraded one[3], as the matrix formed by non-local similar patches in natural images is low-rank[4]. However, the low-rank matrix recovery model is mainly applicable to 2D data, i.e., matrices. However, real-world data is often 3D, such as color images and videos, which are usually represented as 3-order tensors. Compared with 2D image patches, the high-order singular values of 3D cubes have more significant inherent sparsity, which means that the low-rank property of tensors is more prominent than that of matrices [5],[6]. Therefore, to better preserve the multidimensional structure of color images, we introduce the low-rank tensor recovery model to deal with tensor data, which is more suitable for color image restoration tasks.

Due to the non-convexity of rank constraint, the tensor nuclear norm is commonly used as its convex surrogate function[7]. In this paper, the tensor nuclear norm is defined as the sum of higher-order singular values, i.e.,  $\|\mathcal{X}\|_* = \sum_i \sigma_i(\mathcal{X})$ , where  $\sigma_i(\mathcal{X})$  is the  $i$ -th singular value of the core tensor  $\mathcal{S}$ .

The tensor nuclear norm punishes all singular values equally, ignoring the prior knowledge that large singular values correspond to important edge and texture information [8], [9]. Therefore, we adopt the weighted tensor nuclear norm [6]  $\|\mathcal{X}\|_{w,*}$  to more accurately estimate the rank of  $\mathcal{X}$ .

$$\|\mathcal{X}\|_{w,*} = \sum_j w_j \sigma_j(\mathcal{X}), \quad (2)$$

---

This work was supported by the Science and Technology Project of Guangzhou under Grant 202103010003, Science and Technology Project in key areas of Foshan under Grant 2020001006285.

**Table 1.** Average PSNR and SSIM of different nuclear norm-based denoising methods on dataset BSD68. The score marked in bold is the best.

Sigma	Index	Methods				
		Noisy	NNM	WNNM	TNNM	WTNNM
10	PSNR↑	28.133	28.470	33.548	<b>35.409</b>	35.288
	SSIM↑	0.7036	0.7878	0.9184	0.9462	<b>0.9482</b>
30	PSNR↑	18.590	27.457	28.163	29.344	<b>29.500</b>
	SSIM↑	0.3272	0.7633	0.8255	0.8275	<b>0.8407</b>
50	PSNR↑	14.153	20.245	25.679	26.806	<b>26.823</b>
	SSIM↑	0.1884	0.3351	0.7054	0.7167	<b>0.7222</b>

where  $\mathbf{w} = [w_1, \dots, w_n]$ ,  $w_j$  is the non-negative weight corresponding to  $\sigma_j(\mathcal{X})$ . In this paper, the weight is set as:

$$w_j = 2\sqrt{2} * \sigma_n^2 \sqrt{l} / (|\sigma_j(\mathcal{X})| + \epsilon), \quad (3)$$

where  $\sigma_n^2$  is the noise variance of the tensor cube estimated using [10].  $l$  is the number of the nearest non-local cubes.  $\epsilon$  is a very small positive constant to avoid dividing by zero.

Table 1 lists four algorithms for denoising on dataset BSD68 [11], including Weighted Nuclear Norm Minimization (WNNM) [8], Weighted Tensor Nuclear Norm Minimization (WTNNM) [6], as well as Matrix Nuclear Norm Minimization (NNM) and Tensor Nuclear Norm Minimization (TNNM) with weights all set to 1. Through quantitative comparisons of Peak Signal-to-Noise Ratio (PSNR) and structure similarity (SSIM) [12] values, it can be found that the TWNNM method performs best in most cases, indicating the effectiveness of tensor representation and weighting strategy.

### 3. DETAILED SOLUTION OF OUR PROPOSED MODEL

#### 3.1. Weighted Low-Rank Tensor Retinex Model

In this section, we propose a Weighted Low-Rank Tensor Retinex (WLRTR) model for simultaneously estimating the illuminance  $\mathcal{L} \in \mathbb{R}^{I_1 \times I_2 \times 3}$  and reflectance  $\mathcal{R} \in \mathbb{R}^{I_1 \times I_2 \times 3}$  from the observed image  $\mathcal{Y} \in \mathbb{R}^{I_1 \times I_2 \times 3}$ .

As images captured in low-light conditions tend to contain intense noise, which may be exacerbated during the process of enhancement, we employ the robust Retinex model[13], which considers noise  $\mathcal{N} \in \mathbb{R}^{I_1 \times I_2 \times 3}$  as an explicit term:

$$\mathcal{Y} = \mathcal{L} \circ \mathcal{R} + \mathcal{N}. \quad (4)$$

The proposed WLRTR model is represented as follows:

$$\begin{aligned} \arg \min_{\mathcal{R}, \mathcal{L}} & \|\mathcal{Y} - \mathcal{R} \circ \mathcal{L}\|_F^2 + \lambda_1 BTV(\mathcal{L}) + \lambda_2 \|\mathcal{W}_r \circ \nabla \mathcal{R}\|_1 \\ & + \lambda_3 \sum_i \|\mathcal{P}_i \mathcal{R}\|_{\mathbf{w},*}, \end{aligned} \quad (5)$$

where  $\|\cdot\|_*$  is the Frobenius norm [6].  $\lambda_1, \lambda_2, \lambda_3$  are regularization parameters to balance the terms. To effectively extract piecewise smooth illuminance, we directly employ the Bilateral Total Variation (BTV)[14] to facilitate texture smoothing and preserve image structure. BTV exhibits superior discrimination between image texture and structure. It effectively smooths image textures while simultaneously preserving weak structures.  $BTV(\mathcal{L})$  represents the bilateral total variation of the illuminance, and its formula can be found in reference [14].

Besides,  $\nabla$  is a first-order difference operator.  $\mathcal{P}_i$  is an operation that extracts cubes similar to the key cube located at position  $i$ . For a key cube with size  $b \times b \times 3$  in a color image, we search for its  $l$  nearest non-local similar cubes in a local window. Then, we combine these non-local similar cubes into a 3-order tensor of size  $b^2 \times (l+1) \times 3$ .  $\|\mathcal{X}\|_{\mathbf{w},*}$  is the weighted tensor nuclear norm [6] to estimate the rank of  $\mathcal{X}$ . The weight  $\mathbf{w}$  in this paper is determined following reference [6].

We also introduce an illuminance-aware weighting scheme by empirically incorporating a weight tensor  $\mathcal{W}_r = 5e^{-10\mathcal{Y}}$  into the total variation of the reflectance. This scheme enables adaptive denoising across different brightness areas.

By using variable splitting technique [15], objective function (5) can be formulated as the following minimization problem by introducing auxiliary variable  $\mathcal{Z}$ :

$$\begin{aligned} \arg \min_{\mathcal{R}, \mathcal{L}, \mathcal{Z}_i} & \| \mathcal{Y} - \mathcal{R} \circ \mathcal{L} \|_F^2 + \lambda_1 BTV(\mathcal{L}) + \lambda_2 \| \mathcal{W}_r \circ \nabla \mathcal{R} \|_1 \\ & + \lambda_3 \sum_i \left( \frac{1}{\sigma_n^2} \| \mathcal{P}_i \mathcal{R} - \mathcal{Z}_i \|_F^2 + \| \mathcal{Z}_i \|_{\mathbf{w},*} \right), \end{aligned} \quad (6)$$

where  $\sigma_n^2$  is the noise variance of the  $i$ -th tensor cube  $\mathcal{P}_i \mathcal{R}$  estimated using [6].

By replacing  $\mathcal{Z}_i$  in (6) with high-order singular value decomposition (HOSVD)[2] and introducing an auxiliary variable  $\mathcal{T}$ , (6) can be rewritten as:

$$\begin{aligned} \arg \min_{\mathcal{R}, \mathcal{L}, \mathcal{S}_i} & \| \mathcal{Y} - \mathcal{R} \circ \mathcal{L} \|_F^2 + \lambda_1 BTV(\mathcal{L}) + \lambda_2 \| \mathcal{W}_r \circ \nabla \mathcal{R} \|_1 \\ & + \lambda_3 \sum_i (\| \mathcal{P}_i \mathcal{T} - \mathcal{S}_i \times_1 U_1 \times_2 U_2 \times_3 U_3 \|_F^2 + \sigma_n^2 \| \mathbf{w}_i \circ \mathcal{S}_i \|_1) \\ & \text{s.t. } \mathcal{T} = \mathcal{R}. \end{aligned} \quad (7)$$

where  $\mathbf{w}_i$  is the weight vector of singular values for  $\mathcal{Z}_i$ .

The Alternating Direction Method of Multipliers (ADMM) algorithm used in [6] can be used to solve (7). The augmented Lagrangian function of (7) is

$$\begin{aligned} \arg \min_{\mathcal{R}, \mathcal{L}, \mathcal{T}, \mathcal{S}_i} & \| \mathcal{Y} - \mathcal{R} \circ \mathcal{L} \|_F^2 + \lambda_1 BTV(\mathcal{L}) + \lambda_2 \| \mathcal{W}_r \circ \nabla \mathcal{R} \|_1 \\ & + \lambda_3 \sum_i (\| \mathcal{P}_i \mathcal{T} - \mathcal{S}_i \times_1 U_1 \times_2 U_2 \times_3 U_3 \|_F^2 \\ & + \sigma_n^2 \| \mathbf{w}_i \circ \mathcal{S}_i \|_1) + \frac{\rho}{2} \left\| \mathcal{R} - \mathcal{T} + \frac{\mathcal{J}}{\rho} \right\|_F^2, \end{aligned} \quad (8)$$

where  $\mathcal{J}$  is Lagrange multiplier,  $\rho$  is the penalty parameter.

Specifically, in the  $(k+1)$ -th iteration, the variables in equation (8) can be updated alternately as follows:

(1) *Update  $\mathcal{L}$*

$$\mathcal{L}^{k+1} = \arg \min_{\mathcal{L}} \| \mathcal{Y} - \mathcal{R}^k \circ \mathcal{L} \|_F^2 + \lambda_1 BTV(\mathcal{L}) \quad (9)$$

For the solution to this problem, please refer to [14].

(2) *Update  $\mathcal{R}$*

$$\begin{aligned} \mathcal{R}^{k+1} = \arg \min_{\mathcal{R}} & \| \mathcal{Y} - \mathcal{R} \circ \mathcal{L}^{k+1} \|_F^2 + \lambda_2 \| \mathcal{W}_r \circ \nabla \mathcal{R} \|_1 \\ & + \frac{\rho}{2} \left\| \mathcal{R} - \mathcal{T}^k + \frac{\mathcal{J}^k}{\rho^k} \right\| \end{aligned} \quad (10)$$

By using the iteratively re-weighted least squares method as used for solving  $\mathcal{L}$ , this problem can be transformed into the following linear system problem:

$$\begin{aligned} \mathcal{R}_c^{k+1} = & \left( \mathcal{L}_c^{k+1,T} \mathcal{L}_c^{k+1} + \lambda_2 M + \frac{\rho}{2} \mathcal{I} \right)^{-1} \\ & \left( \mathcal{L}_c^{k+1,T} \mathcal{Y} + \frac{\rho^k}{2} \left( \mathcal{T}^k - \frac{\mathcal{J}^k}{\rho^k} \right) \right), \end{aligned} \quad (11)$$

where  $M = D_h^T W_h D_h + D_v^T W_v D_v$ .  $W_h, W_v$  are diagonal matrices by diagonalizing  $\mathcal{W}_{r,c}/\nabla_h \mathcal{R}$  and  $\mathcal{W}_{r,c}/\nabla_v \mathcal{R}$  respectively.

This paper utilizes the preconditioned conjugate gradient method (PCG) [16] to accelerate the solution of  $\mathcal{L}$  and  $\mathcal{R}$ .

(3) *Update  $\mathcal{T}, \mathcal{S}_i$*

$$\begin{aligned} \mathcal{S}_i = \arg \min_{\mathcal{S}_i} & \| \mathcal{P}_i \mathcal{T}^k - \mathcal{S}_i \times_1 U_1 \times_2 U_2 \times_3 U_3 \|_F^2 \\ & + \sigma_n^2 \| \mathbf{w}_i \circ \mathcal{S}_i \|_1 \end{aligned} \quad (12)$$

Let  $\mathcal{P}_i \mathcal{T}^k = \tilde{\mathcal{S}}_i \times_1 \tilde{\mathbf{U}}_1 \times_2 \tilde{\mathbf{U}}_2 \times_3 \tilde{\mathbf{U}}_3$  be the HOSVD of  $\mathcal{P}_i \mathcal{T}^k \in \mathbb{R}^{b^2 \times (l+1) \times 3}$ . Then, the tensor singular value thresholding method [6] can be used to solve (12) as follows:

$$\mathcal{S}_i = \max \left( \tilde{\mathcal{S}}_i - \mathbf{w}_i \sigma_n^2 / 2, 0 \right). \quad (13)$$

After solving for each  $\mathcal{S}_i$ , we can reconstruct the whole auxiliary variable  $\mathcal{T}^k$  by solving the following problem:

$$\begin{aligned}\mathcal{T}^{k+1} = \arg \min_{\mathcal{T}} \lambda_3 \sum_i \|\mathcal{P}_i \mathcal{T} - \mathcal{S}_i \times_1 \tilde{\mathbf{U}}_1 \times_2 \tilde{\mathbf{U}}_2 \times_3 \tilde{\mathbf{U}}_3\|_F^2 \\ + \frac{\rho}{2} \|\mathcal{R}^{k+1} - \mathcal{T} + \frac{J^k}{\rho^k}\|_F^2\end{aligned}\quad (14)$$

The closed-form solution for problem (14) can be obtained by solving the system of linear equations:

$$\begin{aligned}\mathcal{T}^{k+1} = & \left( \mathcal{I} + \frac{\lambda_3}{\rho^k} \sum_i \mathcal{P}_i^T \mathcal{P}_i \right)^{-1} \\ & \left( \mathcal{R}^{k+1} + \frac{J^k}{\rho^k} + \frac{\lambda_3}{\rho^k} \sum_i (\mathcal{P}_i^T \hat{\mathcal{S}}_i) \times_1 \tilde{\mathbf{U}}_1 \times_2 \tilde{\mathbf{U}}_2 \times_3 \tilde{\mathbf{U}}_3 \right).\end{aligned}\quad (15)$$

where  $\mathcal{I}$  is the unit tensor,  $\mathcal{P}_i^T : \mathbb{R}^{b^2 \times (l+1) \times 3} \rightarrow \mathbb{R}^{I_1 \times I_2 \times 3}$  is the inverse operation of  $\mathcal{P}_i$ , which aggregates all the cubes of  $\mathcal{T}$  into the image with the size of  $\mathbb{R}^{I_1 \times I_2 \times 3}$ .  $\sum_i \mathcal{P}_i^T \mathcal{P}_i$  denotes the number of overlapping cubes that cover the pixel location.

#### (4) Update Multiplier

The Lagrangian multiplier is updated as follows:

$$\mathcal{J}^{k+1} = \mathcal{J}^k + \rho^k (\mathcal{R}^{k+1} - \mathcal{T}^{k+1}). \quad (16)$$

The algorithm will stop iterating when any of the following conditions are met:

$$\begin{cases} \|\mathcal{L}^{k+1} - \mathcal{L}^k\|_F^2 / \|\mathcal{L}\|_F^2 \leq \varepsilon \\ \|\mathcal{R}^{k+1} - \mathcal{R}^k\|_F^2 / \|\mathcal{R}\|_F^2 \leq \varepsilon. \end{cases} \quad (17)$$

#### (5) Illuminance Adjustment

After obtaining the illuminance  $\mathcal{L}$  and reflectance  $\mathcal{R}$  estimates, Gamma correction is adopted to the illuminance as in [17, 18] to modify the estimated illuminance. It is important to note that gamma correction is performed in the HSV color space to preserve color information. The Gamma correction of the V channel image  $L_v$  of  $\mathcal{L}$  is defined as  $L'_v = L_v^{\frac{1}{\gamma}}$ , where the parameter  $\gamma$  is empirically set as 2.2. The final enhanced result is represented as

$$\hat{\mathcal{Y}} = \mathcal{L}' \circ \mathcal{R}, \quad (18)$$

where  $\mathcal{L}'$  is obtained by converting the gamma-corrected luminance to the RGB color space.

## 4. EXPERIMENTS

### 4.1. Comparisons with BTReinex Method (November 2023)

The quantitative results are detailed in Table 2, and we will continue to supplement the visual comparison chart in the future

### 4.2. Ablation Study

The denoising performance of our proposed method will be suboptimal if the weighted low-rank tensor (WLRT) and illumination-aware weighting schemes are not employed, as illustrated in Fig.1. This finding confirms the effectiveness of these two schemes for noise reduction. Although applying these schemes may result in a slight reduction in the NIQMC metric, as shown in Table 3, it implies that intense noise is effectively suppressed.

### 4.3. Comparisons with SRRR and LR3M Methods

It is worth noting that the SRRR and LR3M methods require significant computational resources, which makes it difficult for them to run on the VV dataset. Therefore, we only tested their performance on the DICM dataset. The DICM dataset contains 44 low-light images.

As shown in Fig.2, the SRRR and LR3M methods can effectively remove intense noise. However, a drawback of these methods is that they tend to smooth out a significant amount of image details, resulting in poor visual quality and quantitative metrics of the enhanced results, as shown in Fig. 2 and Table 4.

**Table 2.** Quantitative comparison of the average results for each evaluation metric on the unpaired real dataset (175 images) and the paired real dataset LOL-v2 (100 paired images).  $\uparrow$  ( $\downarrow$ ) indicates that a higher (lower) value of the metric corresponds to better image quality. Numbers highlighted in **bold red** and **bold green** correspond to the **best** and **second-best** results, respectively.

Dataset	175 Unpaired Images			LOL-v2	
Metric	NIQE $\downarrow$	NIQMC $\uparrow$	VIF $\uparrow$	PSNR $\uparrow$	SSIM $\uparrow$
<b>Input</b>	5.645	4.508	1.000	15.878	0.568
<b>JieP</b>	3.932	4.983	1.281	17.150	0.586
<b>STAR</b>	3.836	5.001	1.132	13.411	0.508
<b>LR3M</b>	-	-	-	13.411	0.508
<b>PnPRetinex</b>	3.849	5.188	<b>1.468</b>	17.463	0.580
<b>ZeroDCE</b>	<b>3.833</b>	5.066	1.179	18.059	0.603
<b>SCI</b>	5.361	5.190	1.078	17.304	0.555
<b>URetinex</b>	3.950	<b>5.223</b>	1.037	-	-
<b>BTRetinex(2023)</b>	-	-	-	<b>18.171</b>	<b>0.621</b>
<b>WLRTR(Ours)</b>	<b>3.021</b>	<b>5.239</b>	<b>1.483</b>	<b>18.481</b>	<b>0.649</b>



**Fig. 1.** The impact of two schemes. (a) Input. (b) w/o  $\mathcal{W}_r$ . (c) w/o WLRT. (d) WLRTR(Ours)

**Table 3.** The impact of two schemes on the 175 images. The score marked in bold is the best.

Metric	IL-NIQE $\downarrow$	NIQMC $\uparrow$
WLRTR w/o $\mathcal{W}_r$	23.1748	<b>5.1861</b>
WLRTR w/o WLRT	23.0705	5.1789
WLRTR	<b>23.0092</b>	5.1769

**Table 4.** Quantitative performance comparison on dataset DICM with IL-NIQE and NIQMC. The score marked in bold is the best.

Metric	IL-NIQE $\downarrow$	NIQMC $\uparrow$
SRRR[19]	24.9799	5.0268
LR3M[13]	26.5407	5.0263
Ours	<b>22.6202</b>	<b>5.1702</b>

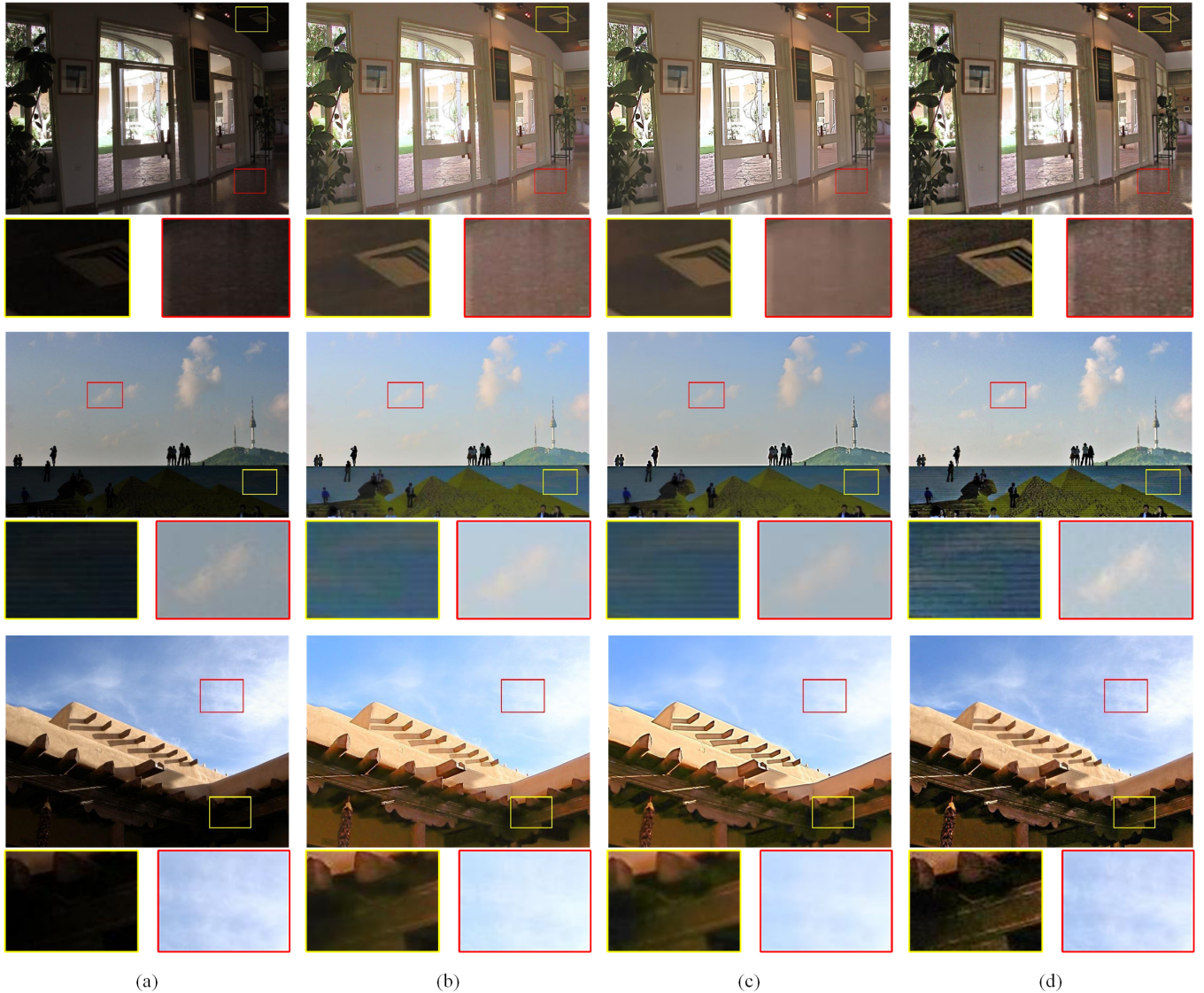


**Fig. 2.** Comparison of enhanced results for low-light images. (a) Input. (b) SRRR. (c) LR3M. (d) Ours.

## 5. REFERENCES

- [1] Tamara G Kolda and Brett W Bader, “Tensor decompositions and applications,” *SIAM review*, vol. 51, no. 3, pp. 455–500, 2009.
- [2] Lieven De Lathauwer, Bart De Moor, and Joos Vandewalle, “A multilinear singular value decomposition,” *SIAM journal on Matrix Analysis and Applications*, vol. 21, no. 4, pp. 1253–1278, 2000.
- [3] Emmanuel J Candès, Xiaodong Li, Yi Ma, and John Wright, “Robust principal component analysis?,” *Journal of the ACM (JACM)*, vol. 58, no. 3, pp. 1–37, 2011.
- [4] Shenlong Wang, Lei Zhang, and Yan Liang, “Nonlocal spectral prior model for low-level vision,” in *Computer Vision–ACCV 2012: 11th Asian Conference on Computer Vision, Daejeon, Korea, November 5–9, 2012, Revised Selected Papers, Part III 11*. Springer, 2013, pp. 231–244.
- [5] Yi Chang, Luxin Yan, and Sheng Zhong, “Hyper-laplacian regularized unidirectional low-rank tensor recovery for multi-spectral image denoising,” in *Proceedings of the IEEE Conference on Computer Vision and Pattern Recognition*, 2017, pp. 4260–4268.
- [6] Yi Chang, Luxin Yan, Xi-Le Zhao, Houzhang Fang, Zhijun Zhang, and Sheng Zhong, “Weighted low-rank tensor recovery for hyperspectral image restoration,” *IEEE transactions on cybernetics*, vol. 50, no. 11, pp. 4558–4572, 2020.
- [7] Maryam Fazel, *Matrix rank minimization with applications*, Ph.D. thesis, PhD thesis, Stanford University, 2002.
- [8] Shuhang Gu, Lei Zhang, Wangmeng Zuo, and Xiangchu Feng, “Weighted nuclear norm minimization with application to image denoising,” in *Proceedings of the IEEE conference on computer vision and pattern recognition*, 2014, pp. 2862–2869.
- [9] Yanchi Su, Haoran Zhu, Ka-Chun Wong, Yi Chang, and Xiangtao Li, “Hyperspectral image denoising via weighted multidirectional low-rank tensor recovery,” *IEEE Transactions on Cybernetics*, 2022.
- [10] Guangyong Chen, Fengyuan Zhu, and Pheng Ann Heng, “An efficient statistical method for image noise level estimation,” in *Proceedings of the IEEE International Conference on Computer Vision*, 2015, pp. 477–485.
- [11] David Martin, Charless Fowlkes, Doron Tal, and Jitendra Malik, “A database of human segmented natural images and its application to evaluating segmentation algorithms and measuring ecological statistics,” in *Proceedings Eighth IEEE International Conference on Computer Vision. ICCV 2001*. IEEE, 2001, vol. 2, pp. 416–423.
- [12] Zhou Wang, Alan C Bovik, Hamid R Sheikh, and Eero P Simoncelli, “Image quality assessment: from error visibility to structural similarity,” *IEEE transactions on image processing*, vol. 13, no. 4, pp. 600–612, 2004.
- [13] Xutong Ren, Wenhan Yang, Wen-Huang Cheng, and Jiaying Liu, “Lr3m: Robust low-light enhancement via low-rank regularized retinex model,” *IEEE Transactions on Image Processing*, vol. 29, pp. 5862–5876, 2020.
- [14] Lei He, Yongfang Xie, Shiwen Xie, and Zhipeng Chen, “Structure-preserving texture smoothing via scale-aware bilateral total variation,” *IEEE Transactions on Circuits and Systems for Video Technology*, 2022.
- [15] Zhouchen Lin, Risheng Liu, and Zhixun Su, “Linearized alternating direction method with adaptive penalty for low-rank representation,” *Advances in neural information processing systems*, vol. 24, 2011.
- [16] Richard Barrett, Michael Berry, Tony F Chan, James Demmel, June Donato, Jack Dongarra, Victor Eijkhout, Roldan Pozo, Charles Romine, and Henk Van der Vorst, *Templates for the solution of linear systems: building blocks for iterative methods*, SIAM, 1994.
- [17] Bolun Cai, Xianming Xu, Kailing Guo, Kui Jia, Bin Hu, and Dacheng Tao, “A joint intrinsic-extrinsic prior model for retinex,” in *Proceedings of the IEEE international conference on computer vision*, 2017, pp. 4000–4009.
- [18] Yi-Hsien Lin and Yi-Chang Lu, “Low-light enhancement using a plug-and-play retinex model with shrinkage mapping for illumination estimation,” *IEEE Transactions on Image Processing*, vol. 31, pp. 4897–4908, 2022.
- [19] Mading Li, Jiaying Liu, Wenhan Yang, Xiaoyan Sun, and Zongming Guo, “Structure-revealing low-light image enhancement via robust retinex model,” *IEEE Transactions on Image Processing*, vol. 27, no. 6, pp. 2828–2841, 2018.